Supplemental Material

Supplemental Material

Supplemental Results: $CHIRTS_{max}$ means and standard deviations

We begin by comparing the means and standard deviations of January, July, and annual $CHIRTS_{max}$ with those from the CRU and MERRA2 (Supplemental Figures 1 and 2, Table 1). These three sources of information provide a reasonably convergent description of the spatial and temporal variations of air temperatures. We observe a reasonable level of correspondence between the three mean fields, with spatial (pattern) correlation values ranging from 0.93 to 0.99 (Table 1). Mean MERRA2 standard deviations were higher than those from the $CHIRTS_{max}$ and CRU data set, which were very similar in magnitude (Table 1) and spatial pattern (Supplemental Figure 2). In some places, the standard deviation of the MERRA2 differed quite substantially from the CRU and $CHIRTS_{max}$ data sets (Supplemental Figure 2). The pattern correlations for the CRU and MERRA2 were lower (~0.5 to 0.9) than the pattern correlations for the CRU and $CHIRTS_{max}$ (~0.9). Note that the $CHIRT_{max}$ is corrected using the CRU standard deviations, but not the $CHTS_{max}$.

We briefly examine differences in the mean $CHIRTS_{max}$ and CRU T_{max} fields (Supplemental Figure 3). A detailed comparison focusing on different parts of the globe will be explored in future analyses. In general, we find that the CHT_{clim} and CRU mean fields are quite similar, but that the spatial resolution of the CHT_{clim} is higher (0.05°) and better suited to support detailed regional analyses. For January, July, and the annual averages, we find that the $CHIRTS_{max}$ is substantially warmer (>5°C) over parts of the Himalayas, while relatively large cold differences are identified over Greenland and north-eastern Asia. The $CHIRTS_{max}$ means are slightly warmer in January (+0.3°C), July (+0.9°C), and over the entire year (+0.7°C). The CRU mean field appears substantially colder in some mountainous regions with relatively low station

densities — like the Himalayas and Andes. The causal factors for these differences will be evaluated in future analyses.

It should be noted that these regions have very low station densities, especially at high elevations. Weather stations in these mountainous areas are almost always preferentially located within valleys. From a statistical perspective, the highest elevations are outside the 'convex hull' of the observations, hence the statistical models must typically project estimates beyond the range of the sampled data. The CRU climatology is based on three-dimensional spline fits to latitude, longitude and elevation. It is possible that the spline fits in these data sparse regions are unreliable. The CHT_{clim}, on the other hand, benefits from the physically-based MERRA2 T_{max} fields – a more direct estimate of Tmax than spline-based elevation transforms. To really address this question, future studies will use dense sets of US validation data with good representation at high elevations. Subsets of this would be representative of sparse networks from the regions like the Himalayas and Andes. Then one would contrast the accuracy of a climatology based on spline fits to elevation with the MWR approach used in this study.

East African Case Study

We present here a brief case study in East Africa, an area afflicted with severe, chronic, and acute food insecurity. While the main purpose of this paper has been to introduce and describe the $CHIRTS_{max}$ process and product, we provide this brief case study to emphasize the value added by $CHIRTS_{max}$. When implemented operationally, the $CHIRTS_{max}$ product should be well-suited to monitoring extremes for three reasons. First, it should be available with fairly short, one-to-two month lag times, suitable for agro-climatic monitoring. Monitoring at these time scales can identify failed growing seasons, supporting the pre-positioning of humanitarian relief. Second, the underlying CHT_{clim} provides high-resolution information that can be useful when

assessing impacts. For example, many crops can be adversely affected when maximum temperatures exceed specific thresholds. Representing local mean temperatures more accurately can improve local assessments of the impacts of temperature extremes. Finally, the additional station data included in the $CHIRTS_{max}$ (Fig. 1A,B and Fig. 4A,B) and the independent TIR-based $CHIRT_{max}$ anomalies should provide additional local information suitable for early warning and impact assessment activities.

The top panels of Supplemental Figure 6 show the 1983 to 2010 mean $CHIRTS_{max}$ and CRU T_{max} estimates. Elevation in East Africa modulates temperature and precipitation, and the region exhibits stark contrasts between moist, cool highlands and hot, dry lowland areas. The mountainous areas of northern Tanzania, western Kenya, and northern and central Ethiopia tend to be wetter and cooler than the surrounding arid lowlands, and are typically heavily populated and relatively agriculturally productive. The low and very warm regions of eastern Kenya, southeastern Ethiopia, and Somalia are typically too dry to support much agriculture. These regions often support pastoralist populations. Millions of people live in areas that are between these climatic extremes — areas that are prone to drought and water stress. The CHT_{clim} helps delineate in detail the temperature gradients associated with these climatic conditions, as well as conditions conducive to specific crops such as maize or coffee. The substantially higher resolution of the $CHIRTS_{max}$ product (top-left Supplemental Figure 6) can help effectively identify these temperature gradients.

As temperatures warm, the gradients of temperature will also shift, potentially changing the "front lines" of climate risk. Many climate risks are associated with extremes as opposed to low frequency changes in means— although the latter, of course, influences the former. To explore the representation of these extremes in $CHIRTS_{max}$ and CRU TS 4.1 data sets, we identified the

71 warmest annual T_{max} value between 2011 and 2016 and plotted the values as anomalies from the
72 1981-2010 mean (bottom Supplemental Figure 6). There is a stark difference in these fields as
73 portrayed by the $CHIRTS_{max}$ and CRU TS 4.1 data sets. Notably, we see very large (for the
74 tropics) temperature anomalies in the $CHIRTS_{max}$ data in populated mountainous agriculturally
75 significant areas of Kenya and Ethiopia. These cool mountainous areas exhibit warm anomalies
76 exceeding +1°C. In contrast, the CRU TS 4.01 places the warmest anomalies in far eastern
77 Ethiopia and Somalia. It is not clear what is driving these extremes, given the limited data
78 entering the CRU.
79 While the local spatial patterns in the CRU and $CHIRTS_{max}$ appear quite different, the
80 regional temporal variations appear quite similar (Supplemental Figure 7). Here, we focus on an
81 area that faces chronic and acute food insecurity (Funk and al. 2019; Funk et al. 2008; Taylor et
82 al. 2011). The left panel in Supplemental Figure 7 shows the current food security situation
83 based on the Famine Early Warning Systems Network Integrated Food Security Phase
84 Classification assessment for October of 2017. Orange and red regions were in a food crisis or
85 emergency. This area is also known to have experienced substantial declines in March-April-
86 May precipitation (Funk et al. 2018). The central panel of Supplemental Figure 7 shows March-
87 April-May precipitation for this area, expressed as standardized precipitation index values. This
88 time series is based on the Centennial Trends archive (1900-1980) (Funk et al. 2015b) and the
89 CHIRPS precipitation data set (1981-2016) (Funk et al. 2015c). The right-hand panel of
90 Supplemental Figure 7 shows time series of annual T_{max} data from the CRU TS 4.01 and the
91 $CHIRTS_{max}$, $CHIRT_{max}$, and $CHTS_{max}$ archives. All the data sets indicate a large and troubling
92 increase of ~+1.2°C between the early 1980s and late 2010s. These magnitudes of the regionally

93 averaged changes are highly congruent. The continued high levels of food insecurity experienced
94 in this region may be related not only to reduced precipitation but also rapid warming.
95
96 **Examples from an early warning context**
97 We present here brief examples drawn from two recent African droughts, using data from
98 the Early Warning eXplorer instance run at the CHC (http://chg-ewxtest.chg.ucsb.edu/). We
99 stress here the utility of $CHIRT_{max}$ and $CHTS_{max}$ as two independent sources of information.
100 Effective early warning systems use convergence of evidence to build confidence and trigger
101 interventions that can save lives and livelihoods. While satellite-gauge precipitation, vegetation
102 indices, microwave soil moisture, and actual evapotranspiration are all important early warning
103 tools, there are currently few global air temperature monitoring data sets. Updated CHIRTS
104 fields should be able to help fill that goal. As an example, we examine July and December
105 anomalies from 2015.
106 The 2015/16 El Niño produced severe global climate disruptions associated with wide-
107 scale increases in terrestrial air temperatures (Blunden and Arndt 2016; Blunden and Arndt
108 2018). Supplemental Figure 8 shows standardized $CHIRT_{max}$ and $CHTS_{max}$ July and December
109 T_{max} anomalies for Africa, Eurasia, the Maritime Continent and Australia. While the agreement
110 is not perfect, there is a very high level of correspondence between the mostly-independent
111 satellite and station products, and both products identify large areas of exceptionally warm air
112 temperatures. We use the term ‘mostly independent’ to refer to the fact that the $CHIRT_{max}$ has
113 been adjusted using CRU data to account for shifts in the geostationary archive. The effect of
114 these shifts can be seen in time series for focus regions in Ethiopia and South Africa.

In July of 2015 extremely warm temperature anomalies stretched across Sudan, Ethiopia, India, and Indonesia; both the $CHIRT_{max}$ and $CHTS_{max}$ identify similar extremes (Supplemental Figure 8A,B). In India, wide-spread drought impacted more than 300 million people (Guha-Sapir et al. 2017). Both terrestrial emission temperatures and Berkeley-GTS station observations indicate extremely warm conditions. Extremely low July rainfall in northern Ethiopia helped trigger a failure of Ethiopia's main crop growing season, leading to widespread food insecurity impacting more than 10 million people (FEWSNET 2015). Supplemental Figure 9 shows time series of $CHIRTS_{max}$, $CHIRT_{max}$ and $CHTS_{max}$ for the Amhara region in northern Ethiopia. All three indicators suggest exceptionally warm conditions in July of 2015. Note that station data is quite limited for this region and that there is less agreement in previous years. During the 1998 El Niño, $CHTS_{max}$ indicates substantial warmth, but not $CHIRT_{max}$. Conversely during 2002 (a known drought year), $CHIRT_{max}$ indicates warm conditions while $CHTS_{max}$ values are neutral.

The time series plot shown in Supplemental Figure 9A also shows the CRU mean fields used to adjust the $CHIRT_{max}$ dataset. These step-like bias corrections were based on the sequence of geostationary Meteosat satellites used to create the $CHIRT_{max}$. Of particular note is the ~+0.5 step between 2007 and 2008, this transition occured when the Meteosat 7 was moved over the Indian Ocean. Within these time periods, the interannual fluctuations of the CHIRTmax is completely driven by changes in surface emission temperatures, and we see a strong correspondence with the completely independent $CHTS_{max}$ data. Over the 2008-2016 time period, when the Meteosat 7 satellite rested over the Indian Ocean, the two datasets exhibited a correlation of 0.8. Over the 1983-2016 period their correlation was 0.7.

By December of 2015, full blown El Niño conditions had developed, and we see (Supplemental Figure 8C,D) wide-spread warm anomalies across Southern Africa, India,

Indonesia and southern Australia. There is a strong correspondence between the $CHIRT_{max}$ and $CHTS_{max}$ anomaly maps. Extremely warm temperatures appear over southern Africa, India, Oceania and southern Australia. Drought and crop production deficits were particularly severe in the maize triangle in the eastern part of the Republic of South Africa, a region that produces most of southern Africa's corn. Both the $CHIRT_{max}$ and $CHTS_{max}$ products indicated severely warm T_{max} values over this region. Station observations are plentiful in South Africa (Figure 4A,B), and we find a $CHIRT_{max}$/$CHTS_{max}$ correlation of 0.8 over the entire period of record, and a correlation of 0.9 over the 2008-2016 time period. The 2015 southern African T_{max} estimates were extremely warm (~+3°C). Southern Africa experienced a severe drought (FEWSNET 2016). The failed South African maize harvest contributed to widespread regional cereal deficits, price increases that helped push more than 25 million people into severe food insecurity.

While attribution analyses of these temperature extremes is beyond the scope of this study, it seems likely that these very warm conditions arose through the interaction of El Niño-induced warming and climate change , with severe water deficits reducing latent heat fluxes, and increasing terrestrial temperatures. In both Ethiopia and South Africa, severe 2015 crop deficits were preceded by several months by temperature extremes that are likely unprecedented in the historic record. $CHIRTS_{max}$, $CHIRT_{max}$ and $CHTS_{max}$ will likely be useful and important tools for monitoring and evaluating these extremes.

Supplemental Figures

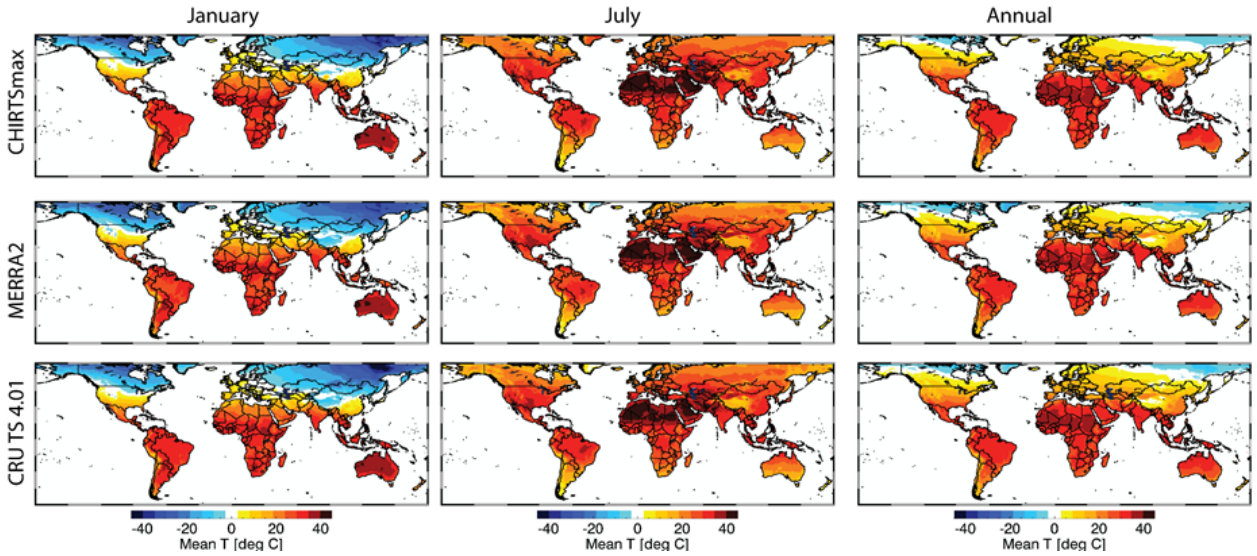

FIG. S1. 1983-2016 mean of $CHIRTS_{max}$, MERRA2, and CRU TS 4.01 monthly T_{max}.

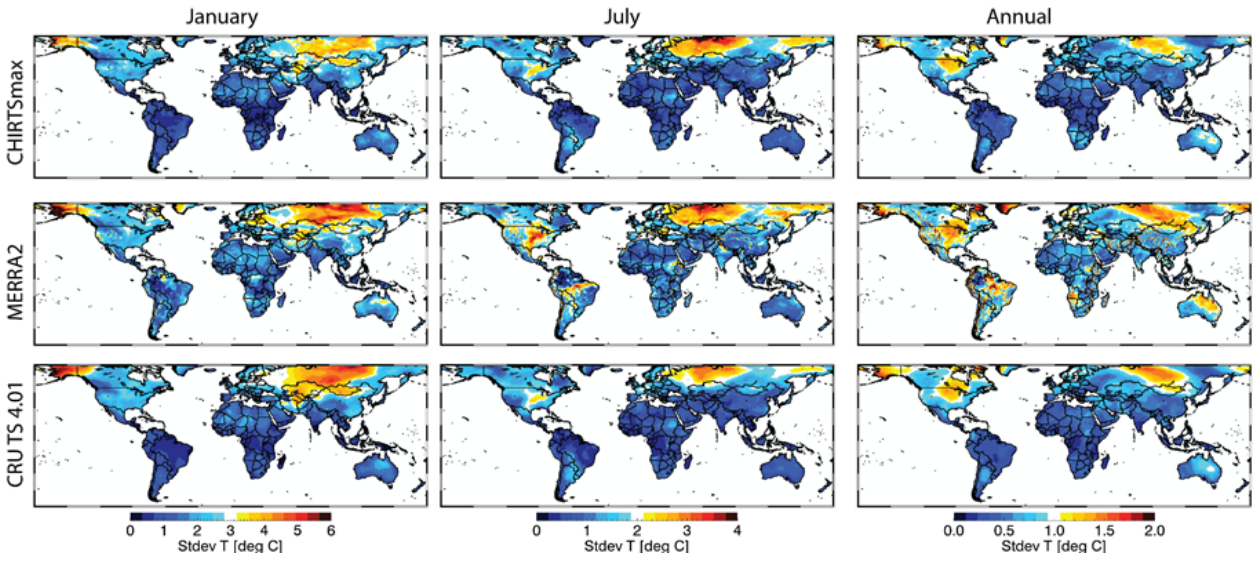

FIG. S2. 2007-2016 standard deviations of $CHIRTS_{max}$, MERRA2, and CRU TS 4.01 monthly T_{max}.

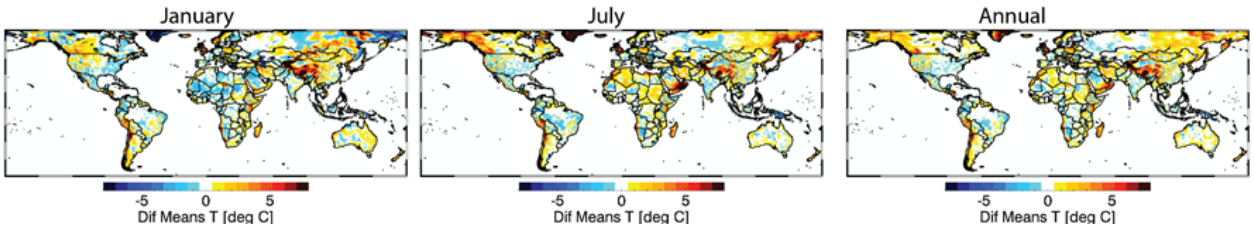

FIG. S3. Differences between January, July and annual $CHIRTS_{max}$ and CRU mean T_{max} temperatures ($CHIRTS_{max}$ minus CRU).

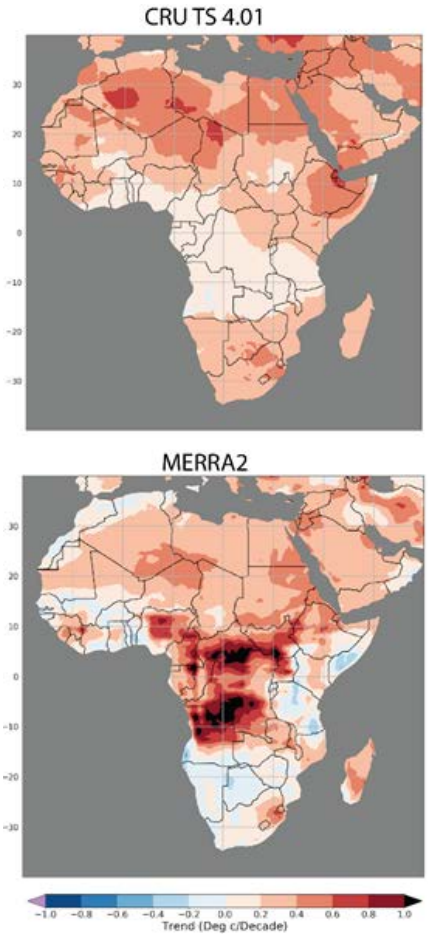

FIG. S4. Kenn-Mandel trend for annual 1983-2016 CRU TS 4.01 and MERRA 2m Tmax estimates.

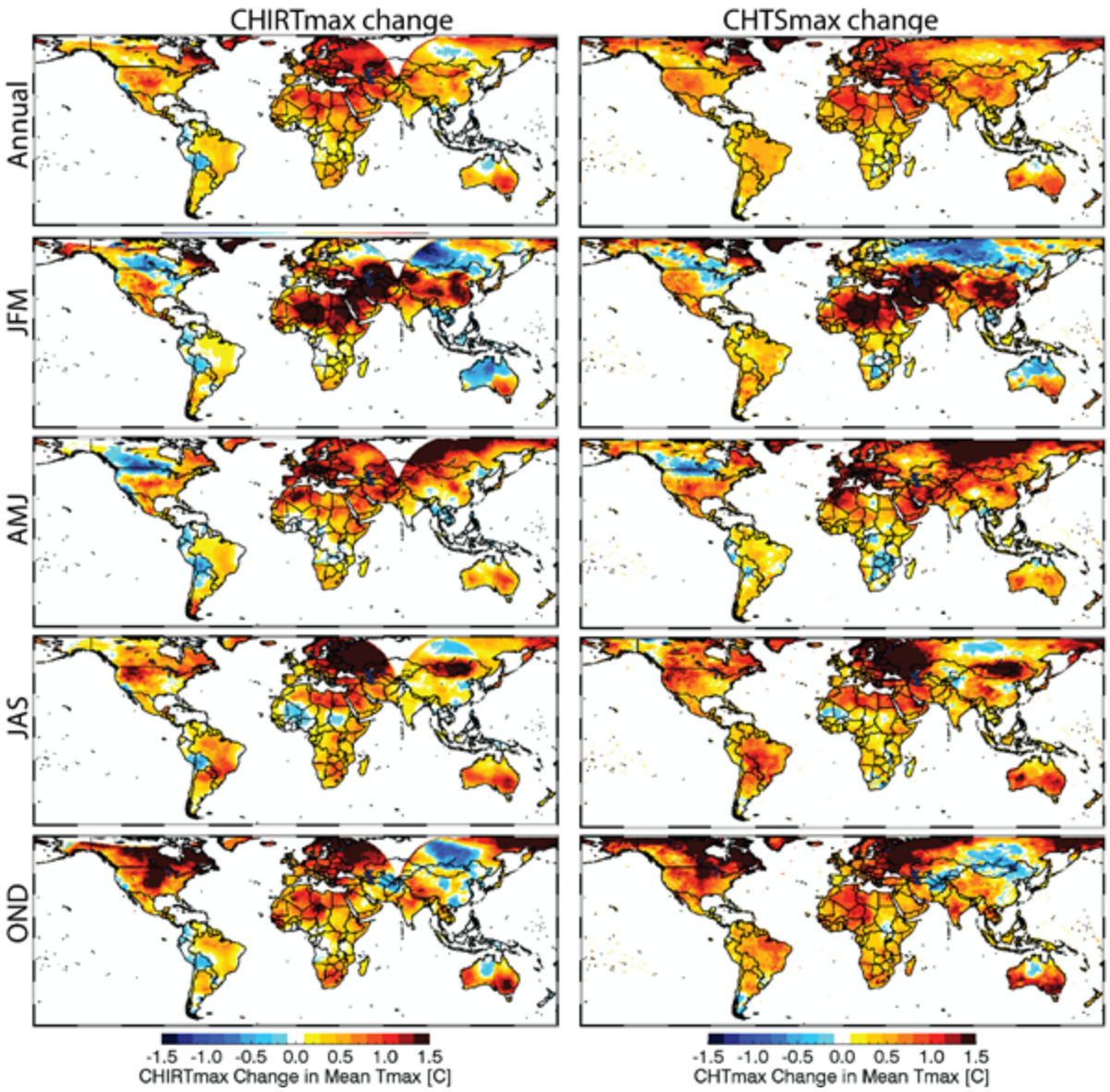

178

179 FIG. S5. Changes in 2001-2016 versus 1983-1998 mean temperatures for the $CHIRT_{max}$ and

180 $CHTS_{max}$ datasets for annual, January-March, April-June, June-September and October-

181 December.

182

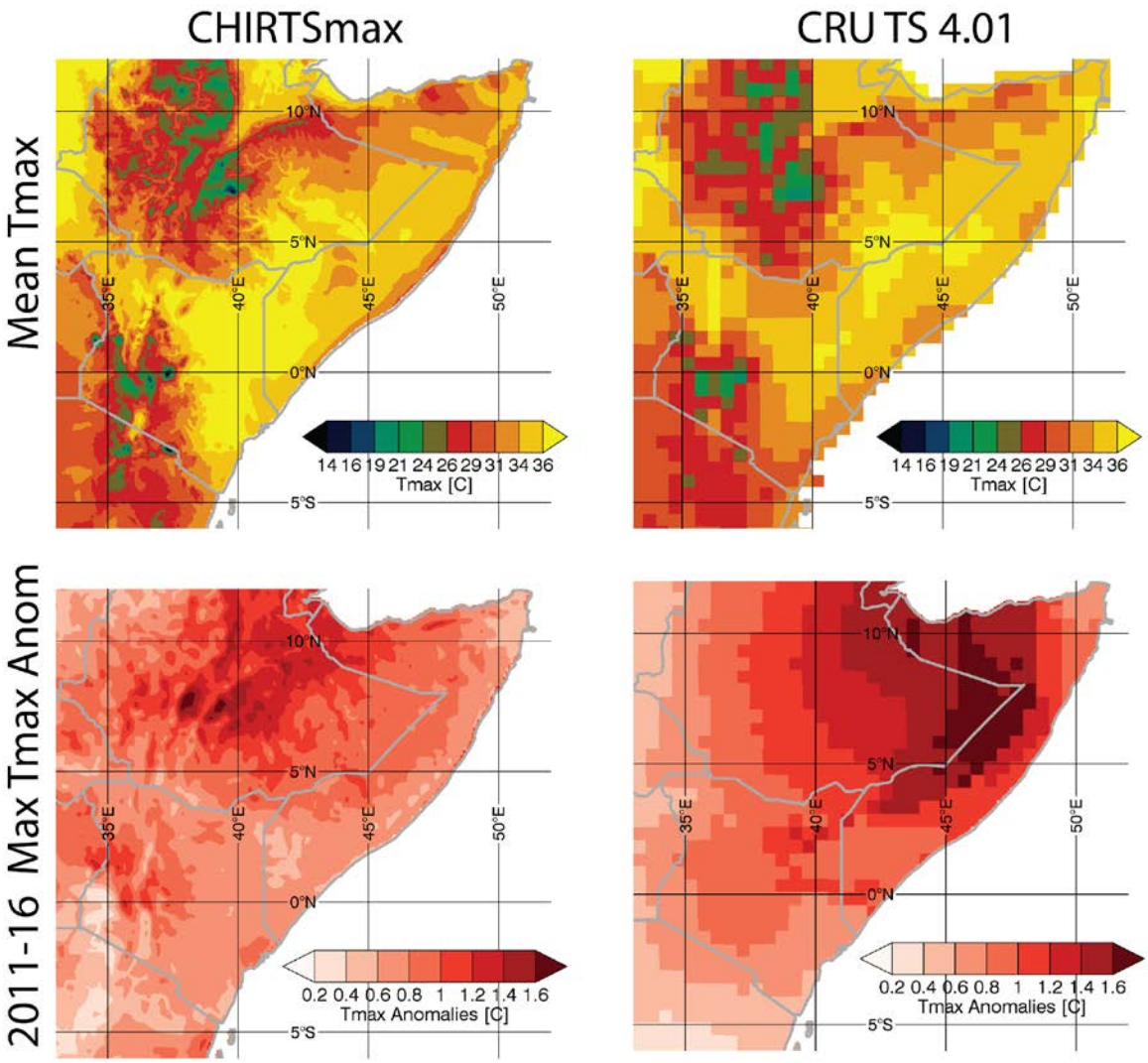

FIG. S6. Mean annual CHIRTSmax (1983-2010) and CRU TS 4.01 (1983-2010) Tmax (top) and the largest 2011-16 annual Tmax anomaly (bottom), based on a 1983-2010 baseline.

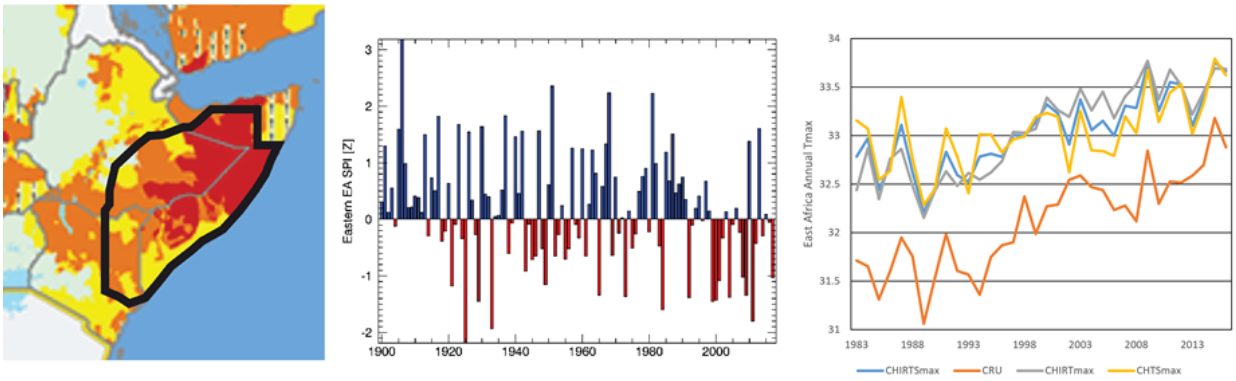

FIG. S7. October 2017 Integrated Phase Classification Food Security Outlook (left), March-May Standardized Precipitation Index time series (middle) and $CHIRTS_{max}$, $CHIRT_{max}$, $CHTS_{max}$ and CRU TS 4.01 annual average T_{max} for the region marked in the left panel (right).

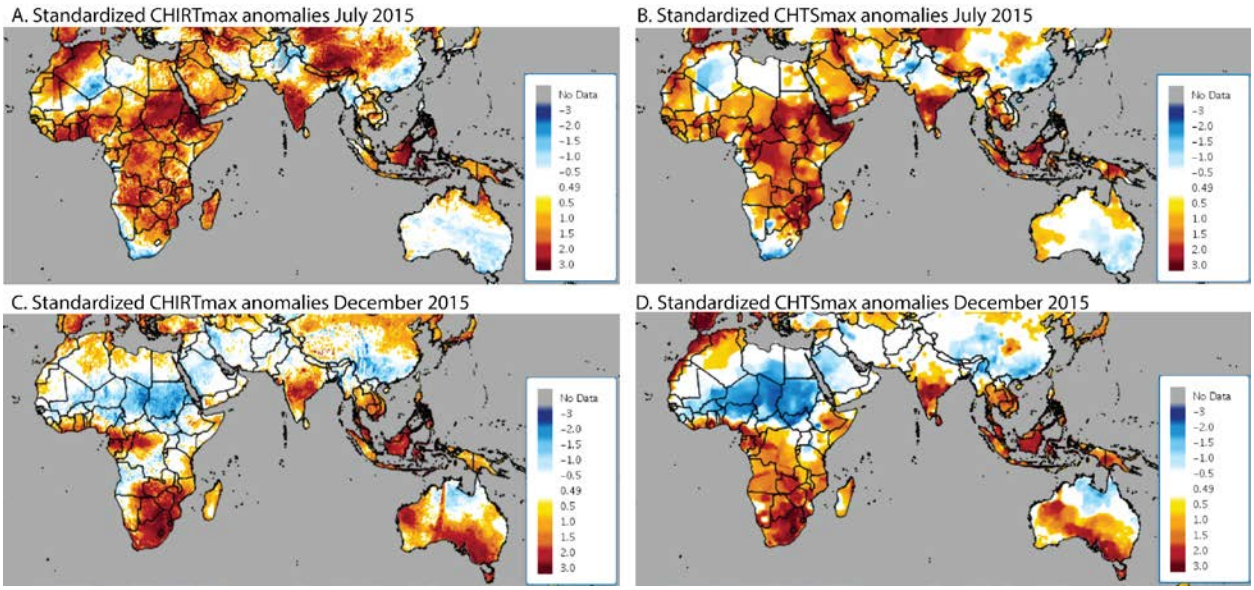

FIG. S8. Examples of monthly $CHIRT_{max}$ and $CHTS_{max}$ standardized anomay maps from the Early Warning eXplorer (EWX). A-B. $CHIRT_{max}$ and $CHTS_{max}$ for July 2015. C-D. $CHIRT_{max}$ and $CHTS_{max}$ for December 2015. Images obtained from http://chg-ewxtest.chg.ucsb.edu/.

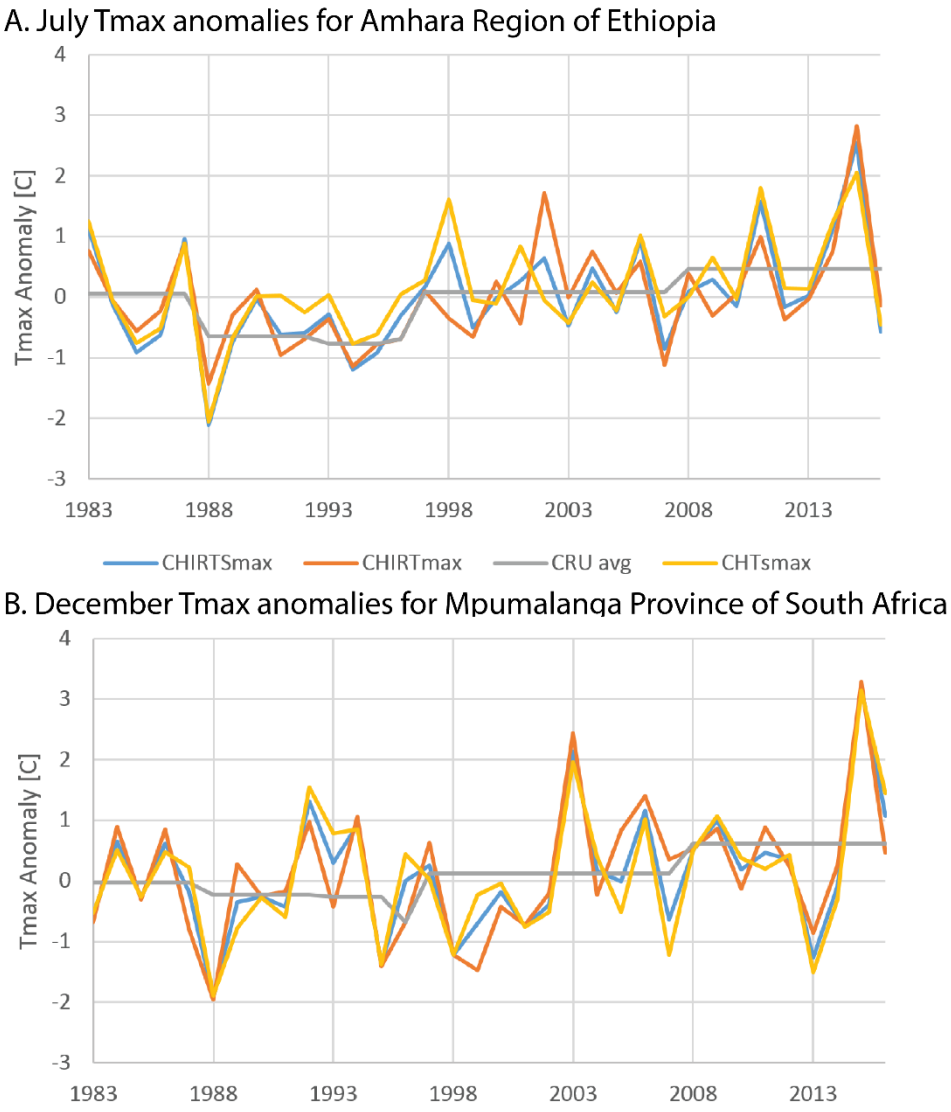

204

205 FIG. S9. Example time series for the Amhara region in Ethiopia (A) and the Mpumalanga

206 Province in the Republic of South Africa (B).

207

208

209

210
211
212 References
213
214 Blunden, J., and D. S. Arndt, 2016: State of the Climate in 2016. *B Am Meteorol Soc*, **98,** Si-
215 S280.
216 Blunden, J., and D. S. Arndt, Eds., 2018: *State of the Climate in 2017*. Vol. 99, Bull. f the Am.
217 Met .Soc., Si–S332 pp.
218 FEWSNET, 2015: Illustrating the extent and severity of the 2015 Ethiopia drought, 7 pp.
219 ——, 2016: Southern Africa - Illustrating the extent and severity of the 2015-2016 drought, 8 pp.
220 Funk, C., and e. al., 2019: Recognizing the Famine Early Warning Systems Network (FEWS
221 NET): Over 30 Years of Drought Early Warning Science Advances and Partnerships Promoting
222 Global Food Security. *Bull. Amer. Meteor. Soc.*
223 Funk, C., M. D. Dettinger, J. C. Michaelsen, J. P. Verdin, M. E. Brown, M. Barlow, and A. Hoell,
224 2008: Warming of the Indian Ocean threatens eastern and southern African food security but
225 could be mitigated by agricultural development. *Proc Nat Acad Sci USA*, **105,** 11081-11086.
226 Guha-Sapir, D., P. Hoyois, P. Wallemacq, and R. Below, 2017: Annual Disaster Statistical
227 Review 2016 - The numbers and trends. Centre for Research on the Epidemiology of Disasters
228 (CRED).
229 Taylor, K. E., R. J. Stouffer, and G. A. Meehl, 2011: An Overview of CMIP5 and the Experiment
230 Design. *B Am Meteorol Soc*, **93,** 485-498.
231
232